

Low-Cycle Fatigue Behavior of Semi-Rigid Top-and-Seat Angle Connections

JOHN B. MANDER, STUART S. CHEN and GOKHAN PEKCAN

ABSTRACT

Constant amplitude reversed cyclic load tests were performed to investigate the low-cycle fatigue behavior of a commonly used class of semi-rigid connection: the top-and-seat angle. All specimens had the same geometrical properties. The test results show that the plastic moment capacity and connection stiffness are sensitive to how the nut and bolts are oriented when tightened. However, upper and lower bounds of strength and stiffness can be predicted using standard yield line (plastic) theory. The variability in strength and stiffness does not appear to affect the fatigue life. Fatigue life predictions can be made for this class of connection using relationships analogous to the well-known Manson-Coffin^{1,2} strain-life equation for metals. Mean rotation (analogous to mean stress) effects are also examined and are shown not to be significant over the range of plastic rotations (0.003 to 0.10 radians) considered. Hysteretic energy-life and energy-rotation relations were also developed. Such relations are useful in seismic damage modeling. For the top-and-seat angle connections considered in this study, the large fatigue based plastic rotation capacity (approx. 3 percent) would generally significantly exceed expected demands for most structural steel systems in a typical US earthquake, where total drift rarely exceeds 2 percent.

1. INTRODUCTION

For seismic design of steel structures the provisions of the AISC-LRFD³ specifications require that design forces resulting from earthquake motions be determined on the basis of energy dissipation in the nonlinear range of response of both members and connections. Since semi-rigid connections, when subjected to moderate or strong earthquakes, become inelastic more quickly than their fully rigid counterparts, consideration of their energy absorption capacity is important. Under seismic ground shaking, the ability of the connec-

tion to dissipate energy will depend on the connection's capability to withstand low-cycle fatigue. Better understanding of the low-cycle fatigue behavior of semi-rigid connections is therefore needed if the structure is to be designed to resist severe reversed cyclic loading.

Consideration of low-cycle fatigue behavior requires the availability of moment-rotation data for connections loaded cyclically to failure. The bulk of available useful data, however, is for connections loaded monotonically, with only a few exceptions.^{4,5,6} Only a few analytical models have been developed for the prediction of cyclic fatigue behavior of semi-rigid joints.^{4,5,7,8,9}

This study constitutes an important step towards the assessment of the seismic vulnerability and damage potential of flexible frames for one specific type of semi-rigid connection. The main focus of this study was to experimentally observe the cyclic and monotonic behavior for a set of identical top-and-seat angle connections, under constant amplitude (drift) cycling. Experimentally obtained data can be used in the investigation of the potential applicability of cumulative damage models, based on energy dissipation as well as plastic connection rotation, for predicting the cyclic response under different types of loading conditions.

2. NOTATION

A	cross-sectional area of column section
b	angle width
d_1	$= h_b + t_f$ (Figure 5(b))
d_2	$= \frac{t}{2} + h_b + k$ (Figure 5(b))
c, d, e, f	coefficient for fatigue relationships
EI_b, EI_c	bending stiffness of beam and column
EI_s	bending stiffness of outstanding leg
EI_t	bending stiffness of vertical leg
f_y, f_{su}	yield and ultimate stress
G	shear modulus
g	distance from heel of angle to the center of fastener hole on vertical leg (Figure 5(c))
g_1	distance between two plastic hinges in the angle on the column leg
g_2	$= d_2 + g_1 - d_1 = g - \frac{H}{2} - \frac{t}{2}$ (Figure 5(b))
H	bolt nut dimension depending on the orientation of the bolt head (Figure 5(b))

John B. Mander is assistant professor, department of civil engineering, State University of New York, Buffalo, NY.

Stuart S. Chen is assistant professor, department of civil engineering, State University of New York, Buffalo, NY.

Gokhan Pekhan is graduate research assistant, department of civil engineering, State University of New York, Buffalo, NY.

h_b, h_c	beam and column depth
k	distance from heel to toe of fillet of angle (Figure 5(c))
K_{je}, K_{jp}	elastic and plastic connection stiffnesses
K_{Te}	overall elastic stiffness
L	distance from point of application of force to the column center line (Figure 6)
L_b, L_c	beam and column lengths
l_{so}	distance from center of rotation to toe of an outstanding leg (Figure 5(b))
m, m_1, m_2, m_3	nominal plastic moment strength per unit length of angle leg
M_{jp}	plastic moment capacity (Figure 7(a))
N_f	fatigue life till incipient failure
N_{ff}	fatigue life till fracture failure
Q	$= K_{jp} / K_{je}$
r	correlation coefficient
R	shape parameter for Menegotto-Pinto equation, also fatigue (R) ratio $= \Delta_{max} / \Delta_{min}$
t_{wc}	column web thickness
t	angle thickness
V_b, V_c	shear force in beam and column
V_{jh}	shear force in the column at the joint
W_f	average hysteretic energy
$W'_{Nf}, W''_{Nf}, W'_{\theta f}$	coefficient for fatigue relationships
α	rotation of the top angle yield line (Figure 5(b))
Δ_{Te}	elastic displacement (Figure 6)
γ_j	shear deformation at the joint
θ_{be}	elastic beam rotation at the joint (Figure 6)
θ_{col}	elastic column rotation at the joint (Figure 6)
θ_{je}, θ_{jp}	elastic, plastic connection rotation (Figure 6)
θ_{jy}	connection rotation at yield (Figure 7(a))
θ_T	total joint rotation ($= \theta_{Te} + \theta_{Tp}$) (Figure 6)
θ_{Te}	elastic component of total joint rotation ($= \theta_{be} + \theta_{col} + \theta_{je} + \gamma_j$) (Figure 6)
θ_{Tp}	plastic component of total joint rotation
θ'_{Nf}	coefficient for fatigue relationship

3. THE TEST SPECIMENS AND SETUP

In this experimental study, since only in-plane response of top-and-seat angle connections was of concern, the experiments were conducted on a structural subassembly. This subassembly represents a typical outer joint of a frame under lateral loads as shown in Figure 1.

The test setup, shown in Figure 1, consisted of a reaction frame supporting an actuator with $a \pm 12$ -in. stroke and 55 kips force capacity. The reaction frame was fixed to the laboratory strong floor. The column section (W8x31) was seated on the strong floor at two points, 8 ft apart (Figure 1). The beam section (W8x21) was mounted on the column flange at the center (i.e., 4 ft apart from the support points), then connected to the actuator with a 51-in. moment arm to the column flange. A Unistrut reference frame bolted to the column ends was used for the drift measurement and also provided the external control for the hydraulic actuator.

Connections contained L6x4x3/8 top-and-seat angles of A36 steel bolted to the beam and column flanges, with a 1-in. thick column flange plate as shown in Figure 2 to minimize the column flange distortion. Specimen and joint details are given in Figure 2. Each angle contained one row of bolts with 3 1/2-in. center-to-center spacing on the 4-in. leg attached to the column flange, and two rows of bolts with 2 1/2-in. center-to-center spacing on the 6-in. leg attached to the beam flange as shown in Figure 2. A325-SC high strength 3/4-in. diameter bolts were used in standard holes together with A325 flat hardened washers under both the head and nut of the bolt, consistent with typical installation procedures involving calibrated wrenches. For the first two tests (2 percent and 4 percent drift) load indicator washers also were used under the nut along with flat hardened washers. It was observed in these tests that proper bolt tensioning required tightening torques of approximately 450 ft-lbs. Therefore, in the rest of the testing program, only A325 hardened flat washers were used with installation torques of 450 ft-lbs. This was considered to apply proper bolt tensioning, as no slip was observed to occur

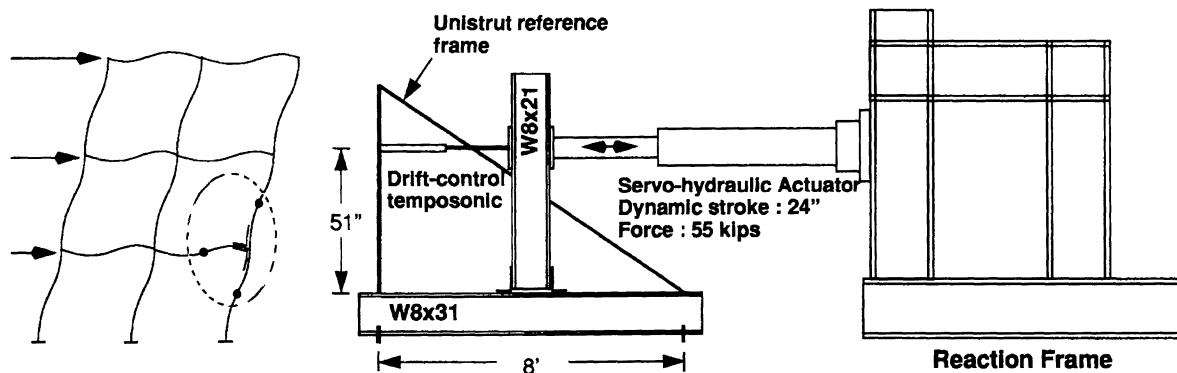


Fig. 1. Test specimens setup.

in any of the tests. Clean mill scale (surface class A) existed on all faying surfaces.

A total of eight coupon tests were conducted to establish the material properties of the angles. Details for the coupon specimens are given in Figure 3. Due to possible anisotropy of the rolled steel in the longitudinal and transverse directions, four of the eight specimens were taken perpendicular to the rolling direction, and the other four along the rolling direction. The average stress-strain curves for the two directions are plotted in Figure 3. The directional dependence was noticeable but not significant. Young's modulus as well as strain hardening modulus was slightly larger for the longitudinal coupon specimens (i.e., specimens that were taken along the rolling direction.). The strain at strain hardening ϵ_{sh} and ultimate strain ϵ_{su} were similar in both directions. The average yield stress of 45.8 and 42.3 ksi and ultimate stresses of 66.6 and 64.7 ksi were obtained for the longitudinal and transverse specimens, respectively.

4. EXPERIMENTAL PROGRAM AND TESTING PROCEDURES

Fourteen identical specimens, all of which were cut from the same stock piece of steel from which the coupons were also taken, were tested under various drift conditions. A summary of experimental parameters is given in Table 1. All of the cyclic tests were conducted until complete fracture of one of the angles occurred.

The specimens were tested cyclically under either equi-amplitude ($R = -1$ where $R = \Delta_{max} / \Delta_{min}$) or one side ($R = 0$) conditions. Eleven equi-amplitude specimens ($R = -1$) were tested at drifts of $\pm 0.6, \pm 0.8, \pm 1.5, \pm 2, \pm 2.5, \pm 3, \pm 4, \pm 5, \pm 6, \pm 7, \pm 8$ percent. Two tests (R0_10, R0_11) were conducted at $R = 0$ for equivalent amplitudes of 2 percent (0 to +4 percent) and 4 percent (0 to + 8 percent) drifts.

The layout of the instrumentation in the joint region is shown in Figure 4. A total of six channels of displacement data were taken; two longitudinally mounted potentiometers were used at the connection to measure displacement related to the connection rotation. Two other potentiometers were

Specimen Id.	R Ratio	Specimen Drift (%)	Cyc. Freq. (Hz.)
M_19	—	12	0.01
R1_08	-1	1.5	0.25
R1_01	-1	2	0.05
R1_07	-1	2.5	0.1
R1_04	-1	3	0.1
R1_02	-1	4	0.05
R1_03	-1	5	0.1
R1_05	-1	6	0.1
R1_09	-1	7	0.1
R1_06	-1	8	0.01
R0_10	0	2	0.1
R0_11	0	4	0.1
R1_12	-1	0.6	1
R1_13	-1	0.8	0.5

transverse to the beam at the connection for an alternate measurement of the connection rotation. A sonic displacement transducer was used in order to provide drift control to the actuator. The applied force was measured by a load cell in the actuator. Data produced by the transducers was recorded after processing by an analog-digital (A/D) converter (Data Translation model DT2801A) mounted in a 486-33 MHz Personal Computer.

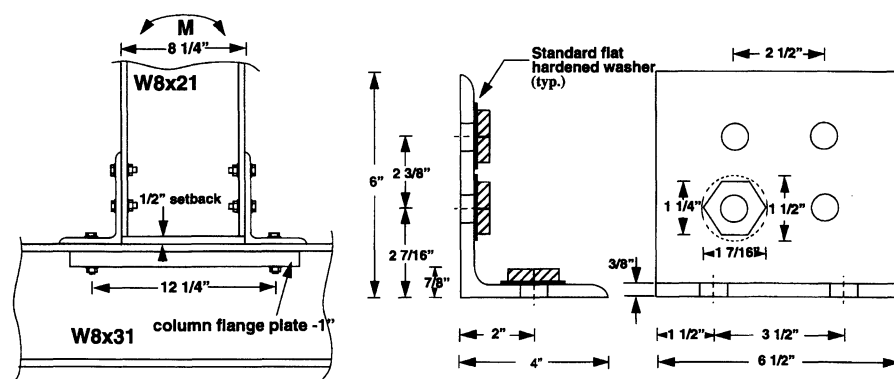


Fig. 2. Connection and test specimen detail.

5. MONOTONIC CHARACTERIZATION

In order to characterize the low-cycle fatigue performance of the test specimens it is first necessary to understand the monotonic behavior and the sources of deformation that contribute to the total drift response.

5.1. Deformation Modeling

The main purpose of this experimental study was to investigate the low-cycle fatigue behavior, which requires the post-elastic behavior to be studied. Therefore, further modeling for the plastic joint rotation is carried out considering the simple mechanism model shown in Figure 5(a). Total joint rotation can be written in terms of its elastic and plastic components as

$$\theta_T = \theta_{Te} + \theta_{Tp} \quad (1)$$

From the geometry of the plastic mechanism (Figure 5(a)), the following relationship can be obtained:

$$\theta_{Tp} = \frac{\theta_{jp} L_b}{L} \quad (2.a)$$

The elastic joint rotation can be defined as follows:

$$\theta_{Te} = \frac{V_b}{K_{Te}} \quad (2.b)$$

Substituting these into Equation 1 and rearranging terms,

$$\theta_{jp} = \left(\theta_T - \frac{V_b}{K_{Te}} \right) \frac{L}{L_b} \quad (3)$$

From Equation 3 it is clear that the plastic rotation of the connection θ_{jp} , is equal to the total drift θ_T , less an amount that is dependent on the peak cycle force (shear force at the connection) V_b and the elastic structural stiffness. In what follows is the determination of the overall elastic stiffness K_{Te} .

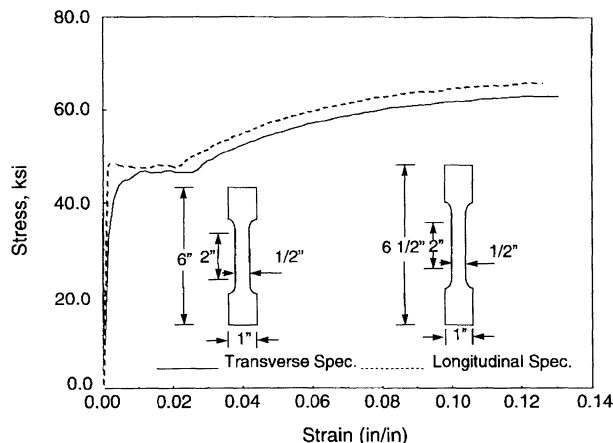


Fig. 3. Coupon test results.

Figure 6 shows the center lines of the beam and column sections and the moment diagram for the given loading. Joint equilibrium requires that

$$V_c L_c = V_b L \quad (4)$$

From the geometry of the deflected shape in Figure 6, it can be shown that the total elastic rotation (drift) of the specimen is given by

$$\theta_{Te} = \frac{\Delta_{Te}}{L} = \theta_{be} + \theta_{col} + \gamma_j + \theta_{je} \quad (5)$$

Rotations due to column and beam deformation are given as follows:

$$\theta_{col} = \frac{V_c L_c^2}{12EI_c} \quad (6)$$

$$\theta_{be} = \frac{V_b L_b^2}{3EI_b} \quad (7)$$

Since the deformation in the panel zone of a joint (γ_j) affects the overall behavior of the connection, this effect is also included in the formulation assuming elastic behavior in the column web. Elastic rotation due to joint panel shear, γ_j , can be easily determined considering the moment diagram in Figure 6. The slope at the joint region, i.e., the joint shear force, is

$$V_{jh} = \frac{\left(V_c \left(\frac{L_c}{h_b} - 1 \right) - \frac{V_b h_c}{2h_b} \right)}{h_b / 2} \quad (8)$$

Using the moment equilibrium given in Equation 4,

$$V_{jh} = V_b \left(\frac{L_b}{h_b} - \frac{L}{L_c} \right) \quad (9)$$

and assuming constant shear force and elastic behavior, the joint panel rotation due to shear can be written as

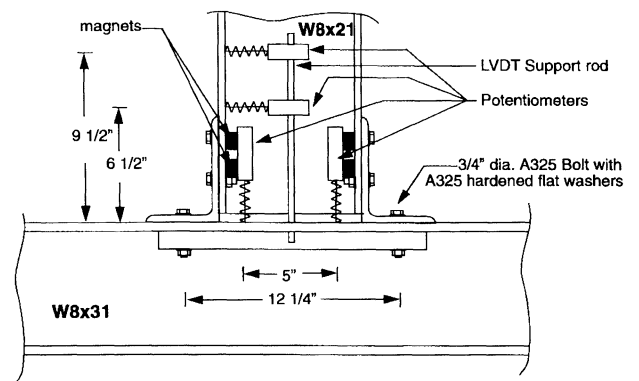


Fig. 4. Joint instrumentation.

$$\gamma_j = \frac{V_{jh}}{AG} = \frac{V_{jh}}{Gt_{wc}h_c} \quad (10)$$

Substituting Equation 9 into 10 and then into 5 yields the total elastic connection rotation as

$$\theta_{Te} = \frac{V_b L_b^2}{3EI_b} + \frac{V_c L_c^2}{12EI_c} + \frac{V_b}{Gt_{wc}h_c} \left(\frac{L_b}{h_b} - \frac{L}{L_c} \right) + \theta_{je} \quad (11)$$

In order to obtain an expression in terms of initial joint and connection stiffnesses, the above equation can be multiplied by $1 / (V_b L_b L)$, noting that $1 / L_b K_{Te} = \theta_{Te} / V_b L_b L$ to obtain

$$\frac{1}{L_b K_{Te}} = \frac{\theta_{Te}}{V_b L_b L} = \frac{L_b}{3EI_b L} + \frac{L_c}{12EI_c L_b} + \frac{1 / (h_b L) - 1 / (L_b L_c)}{Gt_{wc}h_c} + \frac{1}{L K_{je}} \quad (12)$$

After substituting the known geometric parameters into Equation 12 and solving for initial connection stiffness K_{je} , an experimentally inferred connection stiffness may be derived:

$$\frac{1}{(K_{je})_{exp}} = \frac{1.078}{(K_{Te})_{exp}} - \frac{1}{71,250} \quad (13)$$

in which $(K_{Te})_{exp}$ = experimentally obtained initial overall specimen stiffness.

Kishi and Chen^{10,11} have developed an expression for the initial connection stiffness of the top-and-seat angle connection based on kinematic and equilibrium principles, assuming a center of rotation as shown in Figure 5(b). The resulting equation is

$$K_{je} = \frac{4EI_s}{l_{so}} + \frac{3EI_t}{1 + 0.78t_1^2 / g_2^2} \left(\frac{d_1^2}{g_2^3} \right) \quad (14)$$

Subscripts 't' and 's' denote top and seat angle respectively. The critical distance l_{so} is defined as the distance from the plastic hinge at the seat angle (center of rotation) to the tip of the angle leg on beam flange. In this formulation $g_2 = g - H/2 - t/2$ (Figure 5(b)). This equation is used for comparison purposes later in the paper.

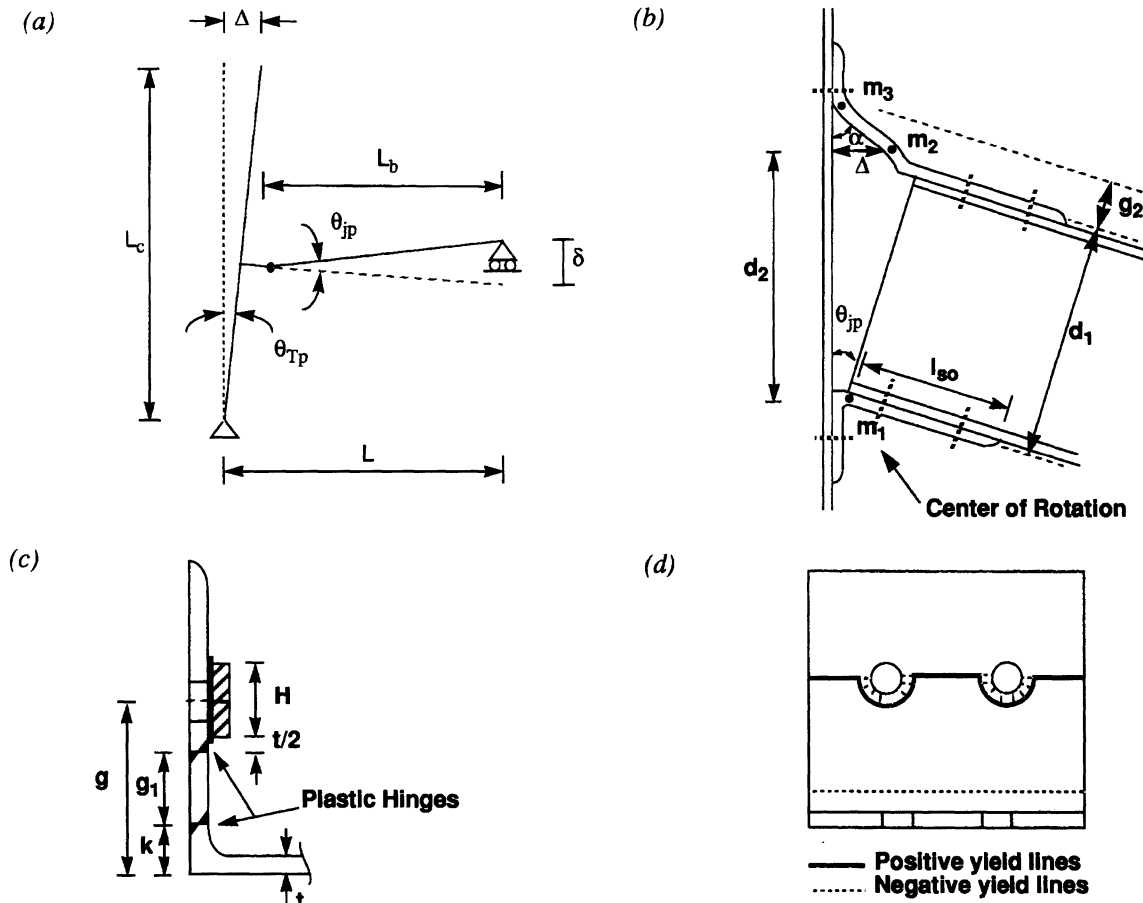


Fig. 5. (a) Plastic mechanism, (b) Definition of parameters-I, (c) Definition of parameters-II, (d) Radial fan yield line pattern.

5.2. Plastic Moment Capacity

The plastic moment capacity of the connection can be determined using virtual work principles based on the plastic hinging in the connection elements as shown in Figure 5(b). External and internal work done can be written as

$$EWD = M_{jp} \theta_{jp} \quad (15)$$

$$IWD = m_1 \theta_{jp} + m_2 (\theta_{jp} + \alpha) + m_3 \alpha = 2m (\theta_{jp} + \alpha) \quad (16)$$

where m_1 , m_2 and m_3 are moment strengths per unit length, all equal to a single value $m (= f_y b t^2 / 4)$ for this case. The rotation of the top-angle yield line from geometry may be defined as,

$$\alpha = \frac{d_2}{g_1} \theta_{jp}$$

Equating Equations 15 and 16 and substituting the known parameters to solve for M_{jp} ,

$$M_{jp} = 2m \left(1 + \frac{d_2}{g_1} \right) = 0.457 f_y \left(1 + \frac{9.3425}{g_1} \right) \quad (17)$$

Note that for the above equation, the plastic mechanism moment capacity of the top-and-seat angle connection is very sensitive to the value of g_1 . To examine the sensitivity of g_1 on the plastic moment capacity three scenarios are explained in what follows:

1. Upper Bound Strength:

If one of the apexes of the bolt head is pointing toward the yield line m_3 (See Figure 5), then the distance g_1 becomes a minimum with the yield line passing directly beneath the hardened washer. However, it should be noted that in the limit as $g_1 \rightarrow 0$, shear capacity rather than the flexural capacity of the angle governs the plastic moment capacity, which yields the following equation:

$$M_{jp} = 2m \left(1 + \frac{h_b + k}{t} \right) = 11.6 f_y \quad (18)$$

For the present specimen this gives $M_{jp} = 491$ kip-in based on $f_y = 42.3$ ksi, and at fracture where $f_{su} = 64.7$ ksi, $M_{jp} = 751$ kip-in.

2. Lower Bound Strength:

If load indicator washers are used, then the yield line m_3 is able to penetrate up underneath the bolt, approaching the center of the bolt hole. In this case,

$$g_1 = g - k = 2 - 0.875 = 1.125 \text{ in.}$$

This gives $M_{jp} = 180$ kip-in.

3. Nominal Plastic Strength:

Post-test inspection revealed that in most cases a radial fan yield line formed beneath the bolt head and washer connect-

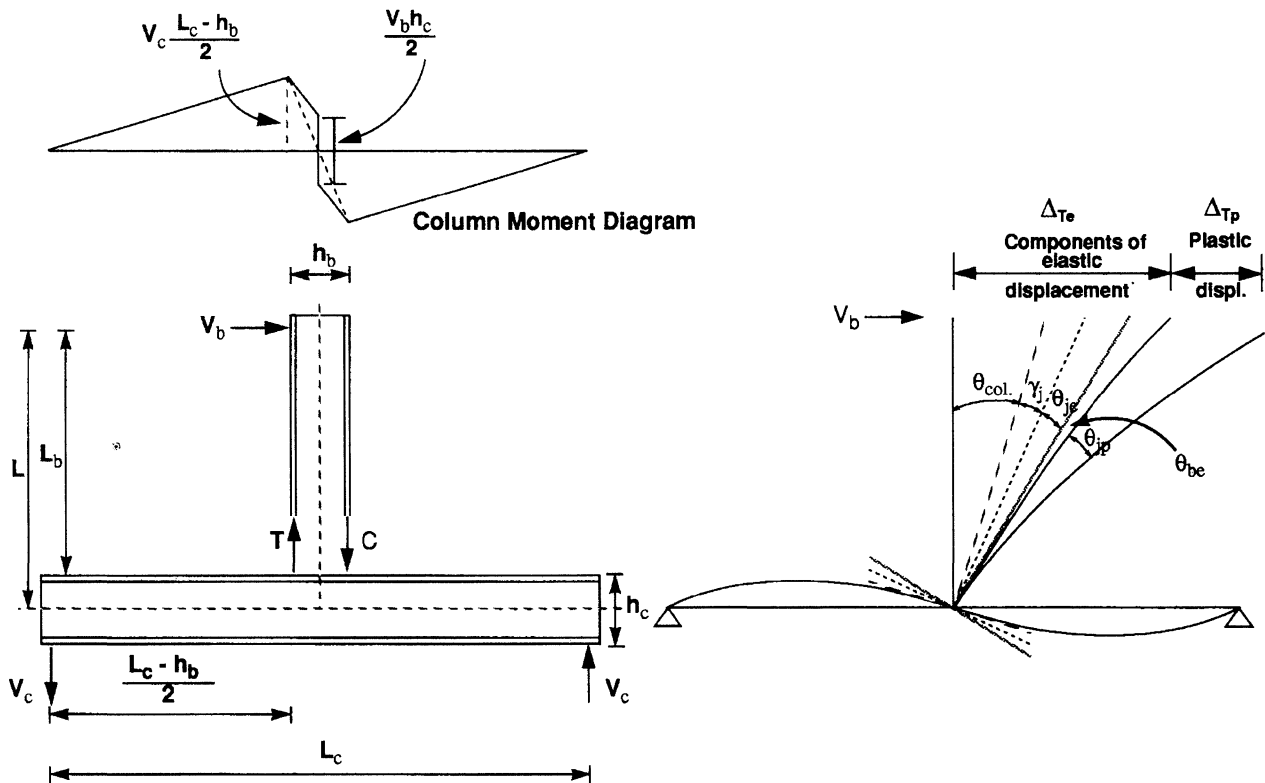


Fig. 6. Free body and deformed geometry.

Table 2.
Summary of Constant Amplitude Cyclic Test Results

Spec Id.	Total Drift (%)	$K_{T\theta}$ kip-in./rad	Expt. K_{je} kip-in./rad	K_{je}^a kip-in./rad	K_{jp} kip-in./rad	Expt. θ_{jp} rad	θ_{jp}^b rad	θ_{JT} rad	M_{jp} kip-in.
M_19	11.85	49 500	122 500	129 300	4 800	0.096	0.107	0.100	337.3
R1_06	8.50	50 900	138 500	140 100	5 700	0.680	0.070	0.071	454.5
R1_09	7.20	48 600	123 600	122 600	5 500	0.570	0.056	0.060	372.5
R1_05	6.10	50 000	137 600	132 900	6 800	0.486	0.045	0.052	504.5
R1_04	3.00	49 400	122 800	128 700	4 500	0.175	0.022	0.022	343.5
R1_01	2.10	44 800	95 300	99 700	5 700	0.107	0.014	0.018	226.1
R0_10	1.98	45 400	93 300	102 900	4 200	0.157	0.017	0.017	267.9
R0_11	4.06	45 900	106 700	105 800	3 600	0.335	0.038	0.036	325.6

a. Inferred experimental value from Equation 13.
b. Experimentally measured using potentiometers.

ing the angles to the column. Such a yield line pattern is shown in Figure 5(d). Using the principles of virtual work for this pattern gave a plastic joint capacity of $M_{jp} = 280$ kip-in.

5.3. Monotonic Behavior

In order to investigate the repeatability and reliability of the monotonic behavior, initial stiffnesses, elastic and plastic rotations from some of the cyclic tests are compared in Table 2. The initial connection stiffness was determined both from the $M-\theta_j$ plots given in Figure 7(a) and using Equation 13. As can be seen from Table 2, initial connection stiffnesses ranged between 138,500 kip-in/rad for specimen R1_06 and 93,500 kip-in/rad for specimen R0_10. However, except for specimens R1_05 and R1_06, connection stiffnesses stayed in an acceptable range, having an average value of 117,500 kip-in/rad. Adopting an average value of g_1 as 1.114 in., the Kishi and Chen¹¹ model of Equation 14 predicts the initial stiffness as 134,500 kip-in/rad. Table 2 also includes the experimentally observed connection mechanism moment M_{jp} for some of the test specimens, ranging between 268 kip-in and 505 kip-in. Comparison with the predicted values confirms that the yield line pattern in the connection angles depends on the bolt head orientation.

5.4. Modeling the Moment-Rotation Behavior

A useful means of describing the monotonic behavior is to use the Menegotto-Pinto¹² (M-P) equation. This is a powerful means for describing a curve between two tangents and has a variable radius of curvature at the intersections. The basic form of the M-P equation for monotonic loading is

$$M = K_{je}\theta_j \left[Q + \frac{1-Q}{\left[1 + \left| \frac{K_{je}\theta_j}{M_{jp}} \right|^R \right]^{1/R}} \right] \quad (19)$$

where R is a curvature parameter which may vary between 1 and 25 (the higher value giving a bilinear curve). The graphical determination of the parameters K_{je} , K_{jp} , θ_{jp} and M_{jp} is shown on Figure 7(a). Strictly the values of K_{je} , M_{jp} , Q and R should be determined using nonlinear regression analysis. However, in view of the significant scatter in the results, K_{je} and K_{jp} (and hence Q) may be determined from the average of a series of experiments, and M_{jp} be found graphically as the intersection of the two tangents (Figure 7(a)). Experimental values for these parameters are assessed in Table 2.

The value for the parameter R may be determined from a graphical construction as shown in Figure 7(a) such that

$$R = \frac{\ln 2}{\ln \left[\frac{1-Q}{(M(\theta_{jy}) / M_{jp}) - Q} \right]} \quad (20)$$

From the present study $(M(\theta_{jy}) / M_{jp}) = 0.72$, thus $R \approx 2$. In Equation 20, the average experimental value of $Q = 0.05$ is used. Figure 7(b) shows the experimentally obtained monotonic $M-\theta_j$ relationships along with the predicted behavior range due to two extreme bolt orientation cases.

In a recent publication by Kishi, et al.,¹³ it was asserted that the Richard and Abbott equation is suitable for describing moment-rotation behavior of semi-rigid connections. This equation is identical to the more general M-P equation, but with $Q = 0$. This conservatively assumes that there is no

strain-hardening in the connection. For comparative purposes the Richard and Abbott equation is shown with the M-P equation in Figure 7(b). It is evident that the top and seat angle connection does indeed exhibit significant strain-hardening which should thus be accounted for in the analytical modeling.

6. EXPERIMENTAL RESULTS OF CYCLIC TESTS

6.1. Equi-Amplitude Tests

The general purpose of the cyclic tests was to quantify the cyclic moment-rotation characteristics and associated low-cycle fatigue behavior of this specific type of top-and-seat angle connection. In order to establish the fatigue-life relationships, constant amplitude test results have been used in the rest of this paper. These relationships are mainly based on the plastic connection rotation as well as energy absorption capacities for predicting the low-cycle fatigue behavior of the connection.

In all of the tests, the same kind of failure mode was observed. The first surface crack occurred on the leg of one of the angles attached to the beam flange, near the toe of the fillet, generally as fine cracks through surface irregularities. A hinge line also formed at the same location on the leg attached to the column flange. For the higher drift tests (> 5 percent) another distinct hinge formation was observed as a line passing through the bolt holes on the leg of the angle on the column flange. The yield line is not a straight line through the angle width in this case, but also forms half circles around the washers together with radial cracks under the washers. Plastic deformation was also observed in “dishing” of the washers seated on the angle leg on the column flange.

Each specimen was tested to complete fracture failure and had similar failure modes. However, for lower drift tests, the fatigue crack extended only through about 70 percent of the angle thickness on the beam flange. In such cases failure was defined as when the moment capacity reduced to a small (but non-zero) value. Elastic panel zone deformation in the joint region was observed to be significant, especially for the higher drift tests. No slip was encountered between the connection elements.

A series of constant, equi-amplitude ($R = -1$) tests were conducted in order to investigate the low-cycle fatigue behavior and to establish a relation between fatigue life and energy dissipated as well as connection rotation for this specific type of connection. Eleven specimens were tested under constant amplitude cyclic loading with complete stress reversals. Two of the tests, R1_12 and R1_13, were conducted in order to clarify the transition from low-cycle fatigue to high-cycle fatigue. $M-\theta$, relationships for some of the specimens are given in Figure 8(a), (b) and (c). A summary of various test results, including the single and cumulative hysteresis loop areas with corresponding fatigue lives, is given in Table 3.

It can be observed from Table 3 that hysteretic energy was almost constant after a few cycles, until the initial fatigue crack occurred. There also appears to be a general trend toward increasing total hysteretic energy accumulation at the longer fatigue life corresponding to the smaller per cycle loop areas. Thus, total hysteretic energy ranged between 206 kip-in for 8 percent drift ($N_f = 0.5$, $N_{ff} = 1.75$) and 10,900 kip-in for 0.6 percent drift ($N_f = 14,461$, $N_{ff} = 17,064$) test. The cycle at which the incipient failure occurred (N_f) was defined in two ways: by visual inspection and as the point at which the hysteretic energy per cycle number drops sharply. All specimens were tested to complete fracture failure (N_{ff} cycles) and had similar failure modes as described earlier.

6.2. Mean Rotation Effects

Generally in fatigue studies, “mean stress and mean strain effects” have been considered, since in reality structures and their components are very rarely subjected to constant equi-amplitude loadings. Therefore, a mean stress or mean strain is usually present. In this experimental study, two tests were

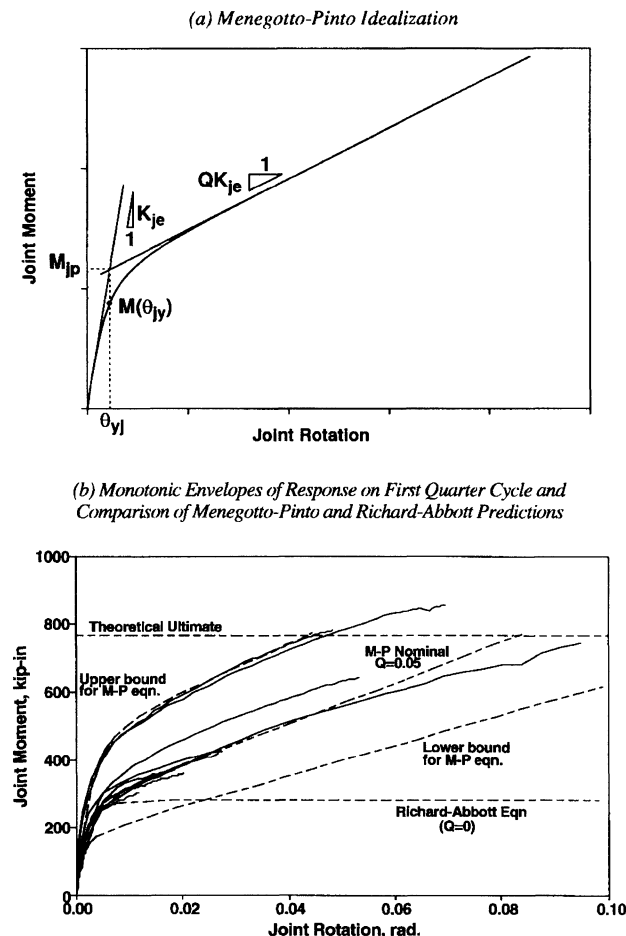


Fig. 7. (a) Menegotto-Pinto idealization (b) Monotonic envelopes of response on first quarter cycle and comparison of Menegotto-Pinto and Richard-Abbott predictions.

Table 3. Specific Test Results					
Spec Id.	% Nominal Drift	Cyc. #	Range of Connection Rotation rad	Area of Single Hysteresis Loop kip-in.	Cumulative Area of Hysteresis Loops ^a kip-in.
R1_06	±8	1	0.1365	119.8	119.8
		1.75	0.1453	86.1	206.0
R1_05	±6	1	0.0987	81.2	81.2
		2	0.1023	69.7	150.9
		3	0.1036	67.4	218.3
		4	0.1101	65.0	295.5
R1_01	±2	1	0.0426	6.8	6.8
		11	0.0423	4.2	54.3
		75	0.0423	4.2	328.5
		95	0.0423	3.0	396.6
R0_11	+8	1	0.0590	33.7	33.7
		2	0.0609	19.4	53.1
		4	0.0622	17.8	88.9
		6	0.0652	20.7	127.4

a. Includes the area under the fractional cycle.

conducted in order to investigate the analogous quantity “the mean rotation” effect, on the low-cycle fatigue behavior of semi-rigid connections. Figure 8(d) shows the experimentally obtained $M-\theta_r$ relationship for specimen R0_11. It should be noted that for these tests an equivalent equi-amplitude rotation is defined as $\theta_j = \frac{1}{2}(\theta_{\max_j} - \theta_{\min_j})$. This is necessary to make a meaningful comparison with equi-amplitude tests.

Based on the observed results in Figure 9, mean rotation effects do not appear to influence the fatigue life of the specimen when compared with similar equi-amplitude tests. This result is consistent with that found by Koh and Stephen¹⁴ for low-cycle fatigue of steel specimens.

7. FATIGUE LIFE MODELING OF THE TEST RESULTS

In experimental low-cycle fatigue studies, the fatigue lives are usually expressed as a function of total or plastic strain. If the strain at critical locations in a structural element could be measured, with a suitable cycle counting method, fatigue lives under random cyclic loading might be predicted accurately, using a regular strain-based Manson¹-Coffin² type of fatigue model. However, being a rather complex system, it is almost impossible and not practical to make strain measurements at the critical locations of a connection. Instead analogous models based on plastic connection rotation are used herein. Thus using the well known Manson¹ and Coffin² relationship the plastic strain amplitude (θ_{jp}) may be related to the number of cycles N_f by:

$$\theta_{jp} = \theta'_{N_f} (2N_f)^c \quad (21)$$

where θ'_{N_f} and c are constants that are unique for a particular connection geometry and $2N_f =$ number of reversals to failure.

The average cyclic energy per cycle ΔW_f , which is measured as the integral area of one hysteresis loop at mid-life ($N_f/2$), can be related to fatigue life,

$$\Delta W_f = W'_{N_f} M_{jp} (2N_f)^d \quad (22)$$

Similarly, the total hysteretic energy can be found from,

$$W_f = W''_{N_f} M_{jp} (2N_f)^e \quad (23)$$

Furthermore, another relationship can be derived relating total work capacity to the constant plastic amplitude by combining Equations 21 and 23,

$$W_f = W'_{\theta_f} M_{jp} \theta_{jp}^f \quad (24)$$

The value of this relationship will become evident when utilized in the damage model described subsequently in the forthcoming paper. In Equations 22 to 24 M_{jp} is used to keep the fatigue relationships independent of size (geometry and material strength).

For the present study the coefficients c , d , e , and f in Equations 21 to 24 were found using linearized (log-log) least squares analysis. It was found that these were close to $c = -1/3$, $d = -0.5$, $e = 0.5$, and $f = -1$. By adopting these results linear regression was used to determine the coefficients θ'_{N_f} , W'_{N_f} , W''_{N_f} , and W'_{θ_f} in Equations 21 to 24. The following fatigue relations were found:

$$\theta_{jp} = 0.070(2N_f)^{-0.333} \quad (25)$$

$$\Delta W_f = 0.303M_{jp}(2N_f)^{-0.5} \quad (26)$$

$$W_f = 0.144M_{jp}(2N_f)^{0.5} \quad (27)$$

$$W_f = 0.0151M_{jp}\theta_{jp}^{-1.0} \quad (28)$$

The fit of the above models to the experimental data is given in Figure 9. Also plotted in Figure 9 are upper and lower bounds for the 95 percentile range. This range was computed assuming normally distributed errors in θ'_{N_f} , W'_{N_f} , W''_{N_f} , and W'_f based on the observed coefficient of variation in those coefficients.

8. DISCUSSION AND IMPLICATIONS FOR SEISMIC DESIGN

The above mentioned fatigue life relationships for this class of semi-rigid connection have been developed based on an analogy with the standard metal fatigue life relationships proposed by Manson¹, Coffin² and Koh and Stephens.¹⁴ The implication from these results for seismic design is that if

plastic hinge rotations are kept below 2 percent then according to Equation 25 at least 50 cycles of complete load reversals can be guaranteed. Furthermore, based on the recent fatigue analysis work carried out at SUNY at Buffalo,^{15,16} it can be shown that the equivalent number of equi-amplitude inelastic cycles at the maximum response displacement that may be expected for metal structures in a typical US earthquake is $N_f = 7$. Thus, from Equation 25 the maximum plastic rotation capacity for such top-and-seat angle connections considered in this study is 0.029 radians. This large fatigue-based rotation capacity would generally well exceed expected demands for most structural steel systems where total drifts rarely exceed 2 percent.

Real earthquake response, however, produces variable amplitude behavior of the members. One way in which seismic induced damage can be assessed is to compare hysteretic energy capacity to hysteretic demand induced by the earthquakes. Therefore, three energy based relationships were derived using the experimental data obtained in the present study.

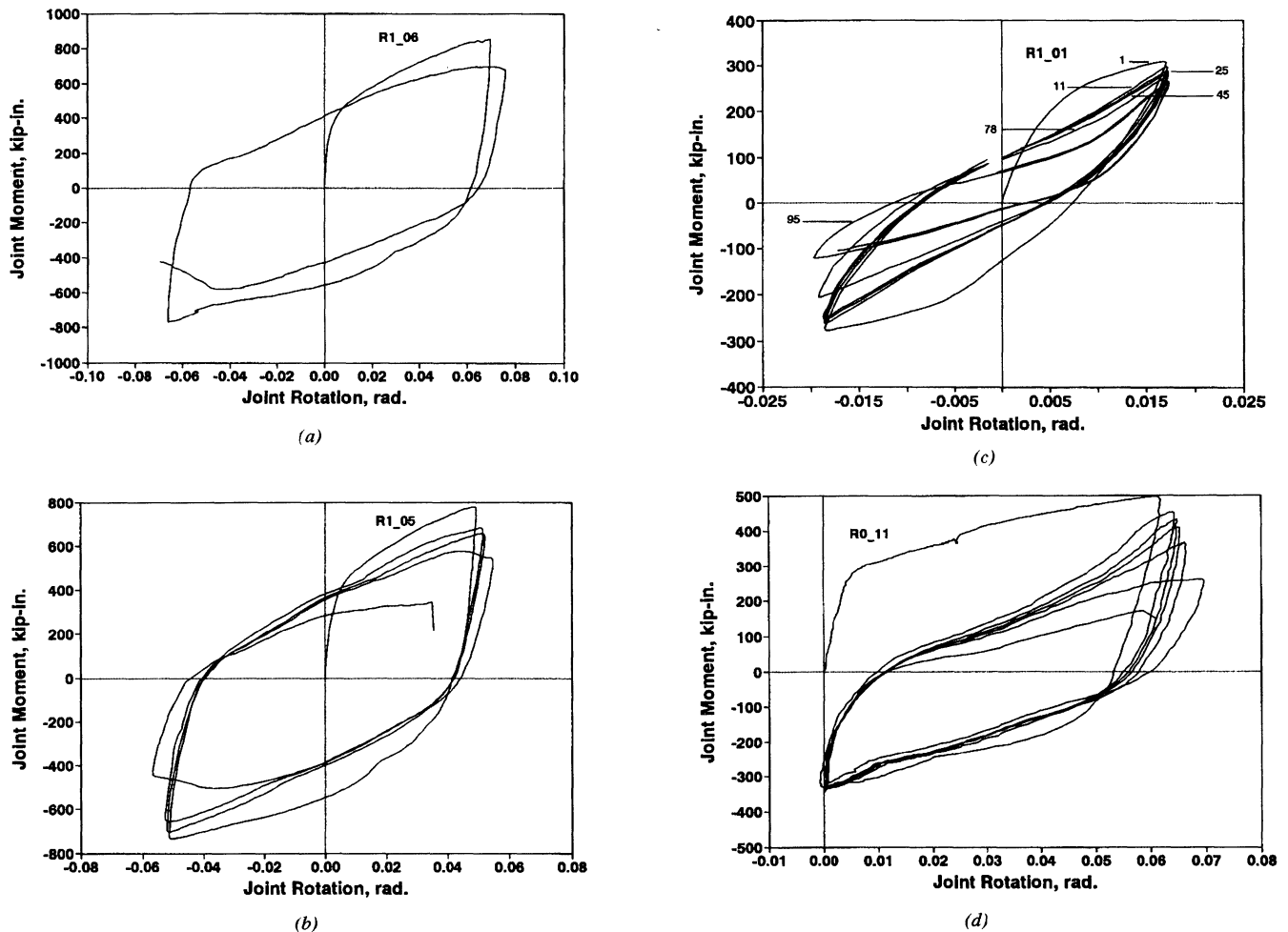


Fig. 8. Hysteresis loops, (a) Specimen R1_06, (b) Specimen R1_05, (c) Specimen R1_01, (d) Specimen R0_11.

The utility of these relationships will be demonstrated in a forthcoming paper on the variable amplitude behavior of semi-rigid top-and-seat angle connections.

9. CONCLUSIONS

The experimental study reported herein was conducted to investigate the low-cycle fatigue behavior of a specific type of semi-rigid top-and-seat angle connection. The following conclusions are drawn:

1. It has been observed that the low-cycle fatigue strength is mainly dependent on three variables: number of cycles of loading, the amplitude of inelastic cycling and the connection geometry.
2. Although each specimen had essentially identical material properties the resultant apparent strength and stiffness varied markedly. A comparison of the experimentally observed values to analytically predicted values has shown that initial connection stiffness and plastic mo-

ment capacity are very sensitive to the first (monotonic) yield line location due to the fact that the orientation of the bolt head and/or nut, washer had a considerable effect on the failure mode and on the plastic hinging in the connection elements. Upper and lower bounds of strengths were obtained applying virtual work principles to the experimentally observed failure modes. This implies that the capacity of semi-rigid bolted connections could be more reliably controlled if the location of hinging in the angle adjacent to the column is fixed. It should be noted, however, that the fatigue life appears to be independent of the nut orientation.

3. Fatigue life relationships for this class of semi-rigid connection were developed based on analogous standard metal fatigue-life relationships in terms of stress, strain and energy.^{1,2,14} The seismic fatigue limited plastic rotational capacity is in the order of 3 percent; this is well in excess of the maximum demands where total structural drifts rarely exceed 2 percent.

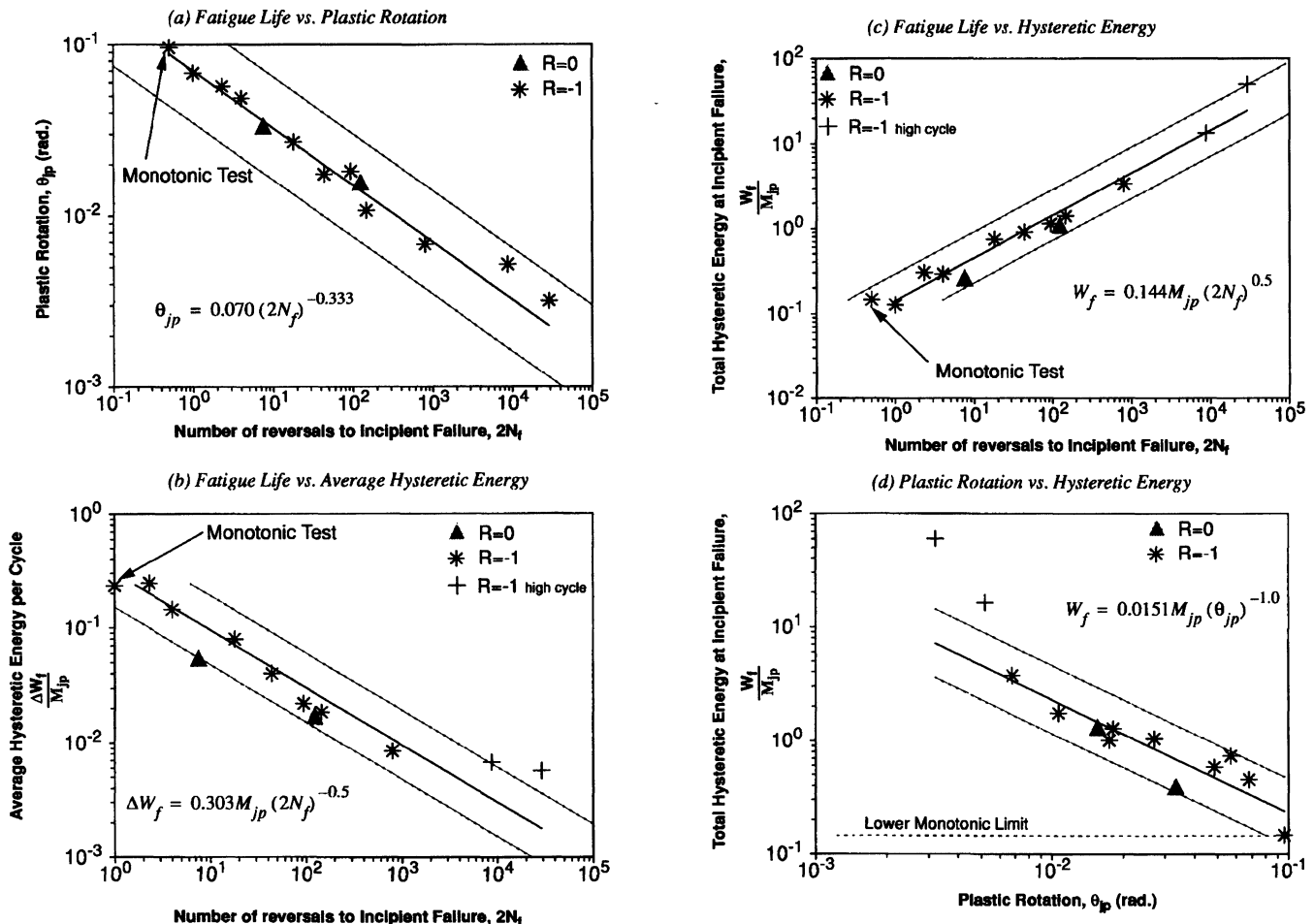


Fig. 9. Fatigue models, (a) Plastic rotation vs. fatigue life, (b) Average hysteretic energy vs. fatigue life, (c) Total hysteretic energy vs. fatigue life, (d) Total hysteretic energy vs. plastic rotation.

ACKNOWLEDGMENTS

Assistance in testing some of the specimens was provided by several graduate students in the Metal Structures course in the Department of Civil Engineering at SUNY at Buffalo. Specimens were donated by Mr. T. Latona of Buffalo Structural Steel Corporation. Partial financial support was provided by the National Center for Earthquake Engineering Research (NCEER) headquartered at SUNY at Buffalo. NCEER technicians Mark Pitman and Dan Walch assisted in the setup and testing. Their help is gratefully acknowledged.

REFERENCES

1. Manson, S. S., "Behavior of Materials under Conditions of Thermal Stress," *Heat Transfer Symposium, University of Michigan Engineering Research Institute*, 1953, pp. 9-75.
2. Coffin, L. F., Jr., "A Study of the Effects of Cyclic Thermal Stresses on a Ductile Metal," *Trans. ASME*, Vol. 76, August 1954, pp. 931-950.
3. American Institute of Steel Construction, *Load and Resistance Factor Design Specification for Structural Steel Buildings*, Chicago, 1986.
4. Azizinamini, A., Bradburn, J. H., and Radziminski, J. B., "Static and Cyclic Behavior of Semi-Rigid Steel Beam-Column Connections," *Technical Report*, Dept. of Civil Engineering, University of South Carolina, March 1985.
5. Harper, W. L., Jr., Dickerson, J. R., Bradburn, J. H., and Radziminski, J. B., "Static and Cyclic Behavior of Semi-Rigid Bolted and Welded Beam-Column Connections," *Structural Research Studies, Technical Report*, Dept. of Civil Engineering, University of South Carolina, May 1990.
6. Astaneh, A., Nader, M., and Malik, L., "Cyclic Behavior of Double Web Angle Connections," *Journal of Structural Engineering*, Vol. 115, No. 5, pp. 1101-1118, 1989.
7. Chasten, C. P., Fleischman, R. B., Driscoll, G. C., and Lu, L. W., "Top and Seat Angle Connections and end-plate connections: behavior and strength under monotonic and cyclic loading," *Proceedings, 1989 National Steel Construction Conference*, AISC, Nashville, TN., pp. 6-1 to 6-32.
8. Dunai, L., and Lu, L. W., "Analytical Modeling of Cyclic Behavior of Bolted Semi-Rigid Connections," in Bjor-

9. hovde, R., ed., *Connections in Steel Structures II: Behavior, Strength, and Design*, AISC, 1992.
10. Huang, J., and Morris, G., "Analysis of Flexibly Connected Frames under Non-Proportional Loading," in Bjorhovde, R., ed., *Connections in Steel Structures II: Behavior, Strength, and Design*, AISC, 1992.
11. Kishi, N., and Chen W., F., "Moment-Rotation Relation of Top-and-Seat Angle Connections," *Structural Engineering Report No. CE-STR-86-26, School of Civil Engineering, Purdue University*, 1986, West Lafayette, Ind.
12. Kishi, N., and Chen W., F., et al., "Moment-Rotation Relation of Top-and-Seat Angle with Double Web Angle Connections," *Proceedings of the State-of-the-Art Workshop on Connections and the Behavior, Strength and Design of Steel Structures, Ecole Normale Supérieure de Cachan, France*, May 25-27, 1987, Elsevier, London, pp. 121-134.
13. Menegotto, M. and Pinto, P. E., "Method of Analysis for Cyclically Loaded Reinforced Concrete Plane Frames Including Changes in Geometry and Non-elastic Behavior of Elements Under Combined Normal Forces and Bending," *IABSE Symposium on the Resistance and Ultimate Deformability of Structures Acted on by Well-Defined Repeated Loads*, Lisbon, 1973.
14. Kishi, N., Chen, W. F., Goto, Y., and Matsuoka, K. G., "Design Aid of Semi-rigid Connections for Frame Analysis," *AISC Engineering Journal*, Third Quarter, 1993, Vol. 30, No. 3, pp. 90-107.
15. Koh, S. K., Stephens, R. I., "Mean Stress Effects on Low-Cycle Fatigue for a High Strength Steel," *Fatigue Fracture of Engineering Materials and Structures*, Vol. 14, No. 4, pp. 413-428, 1991.
16. Mander, J. B., Panthaki, F. D., and Chaudhary, M. T., "Evaluation of Seismic Vulnerability of Highway Bridges in the Eastern United States," *Lifeline Earthquake Engineering in the Central and Eastern U.S.*, ASCE Technical Council on Lifeline Earthquake Engineering, No. 5, pp. 72-86, 1992.
17. Chang, G. A., "Seismic Energy Based Damage Analysis of Bridge Columns," Ph.D. Dissertation, Department of Civil Engineering, State University of New York at Buffalo, July 1993.